Design and Finite Element Analysis of a Novel Reverse Salient Pole Permanent Magnet Synchronous Motor

Xianming Deng, Shusheng Gong, Ran Li, and Junhong Zhou

Jiangsu Province Laboratory of Mining Electric and Automation
China University of Mining and Technology, Xuzhou, 221116, China
xmdengcumt@126.com, shushenggong@cumt.edu.cn

Abstract ─ Since traditional permanent magnet synchronous motor (PMSM) with salient pole effect has a lower d- than q-axis inductance, the maximum torque has a power angle higher than 90 degrees, which poses threat to demagnetization when the motor runs under load. To solve the problem, a novel PMSM with reverse salient pole is designed and optimized to realize the characteristic of $L_d > L_q$ in this paper. Firstly, the electromagnetic design of reverse salient pole PMSM is carried out, followed by finite element analysis (FEA) of traditional PMSM and reverse salient pole PMSM. The simulation results show that air-gap flux density and no-load back EMF of reverse salient pole PMSM is closer to sinusoidal wave compared with the traditional PMSM. The danger of permanent magnet demagnetization is reduced due to $L_d > L_q$. In addition, reverse salient pole PMSM improves the maximum torque and overload capacity and has less loss and higher efficiency in steady-state operation. Finally, the optimal design of reverse salient pole PMSM is carried out. From the comparison of the simulation results, the optimized structure is superior to reverse salient pole PMSM in these performances, which shows that the design is reasonable.

Index Terms ─ Finite element analysis (FEA), PMSM, reverse salient pole, the optimized reverse salient pole.

I. INTRODUCTION

Permanent magnet synchronous motor (PMSM) has been widely used and researched in the industrial field due to high efficiency and high power density. In the analysis and design of PMSM, researchers at home and abroad have done a lot of work and achieved stage results. A lot of work has been done on motor structure and parameter design, which laid the foundation for the design and research of PMSM [1]. A controllable flux PMSM with built-in hybrid rotor magnetic circuit structure was proposed to improve the air-gap flux density waveform, which provides ideas for improving the speed regulation performance of the motor [2]. Optimize the rotor structure by grooving the rotor surface of interior PMSM, reducing the cogging torque of the motor [3].

Recently, a new type of PM motor with the characteristic of $L_d > L_q$, often named a flux-intensifying interior PM (FIIPM) motor, has been proposed and investigated [4, 5]. In addition, Xiaoyong has also carried out a lot of simulations and experiments on permanent magnet Flux-Intensifying Motors [6, 7]. The most obvious characteristic is that the d-axis inductance L_d is greater than the q-axis inductance L_q by the modification of rotor topology. In this paper, reverse salient pole effect of $L_d > L_q$ is realized by changing the rotor structure on the basis of the traditional PMSM. This not only reduces the demagnetization risk of permanent magnets under load operation, but also reduces the saturation degree of rotor magnetic circuit. Next, FEA of traditional PMSM and reverse salient pole PMSM are carried out. The simulation results show that the air-gap flux density and no-load back EMF of reverse salient pole PMSM are closer to sinusoidal wave and have stronger overload capability. In addition, in the starting process, reverse salient pole PMSM can reach the stable operation state more quickly, with less loss and higher efficiency in the steady state. Furthermore, the reverse salient pole PMSM is optimized. The results of FEA show that the optimized structure is superior to the reverse salient pole motor in these performances, which proves the rationality of the structure design.

II. ELECTROMAGNETIC DESIGN OF THE REVERSE SALIENT POLE PMSM

A. Basic parameters design of motor

Basic parameters include the main size of motor, the size and working point of permanent magnet, slot and stator winding. If the slot type is not suitable or electric load is not satisfied, it is necessary to adjust the size of permanent magnet and its correspondence parameters to meet design requirements and technical and economic indicators.

The main dimensions of the motor are the inner and outer diameters of stator and rotor, the stator core length

Submitted On: December 21, 2018
Accepted On: April 6, 2019

and the effective length of air-gap, etc. The main dimensional relationship of the induction motor can be approximated by using to derive the main size relations of the motor. Selected main parameters of motors are shown in Table 1 below.

Table 1: Main parameters of the motor

Parameters	Value
Rated power/kW	20
Rated speed/rpm	1000
Rated line voltage/V	380
Frequency/Hz	50
Stator outer diameter/mm	400
Stator inner diameter/mm	285
Core length/mm	210
Number of poles	3
Stator slot number	72
Rotor slot number	54
Magnet type	NdFe35
Steel type	D23_50

B. Design of rotor structure

Rotor structure design mainly includes the selection of rotor slot shape, the determination of slot size, the determination of permanent magnet type and size, etc. The slots of PMSM rotor with traditional structure and reverse salient pole structure are trapezoidal slots with the same slot size.

$$L=\frac{\psi}{I}=\frac{N\Phi}{I}=\frac{NF}{I\Lambda}=\frac{N\cdot NI}{I\Lambda}=\frac{N^2}{\Lambda}. \quad (1)$$

In (1), ψ is the winding flux, N is the number of winding turns, F is the magnetic motive force, I is the current in the coil, and Λ is the magnetic reluctance.

Formula (1) shows that the inductance is proportional to magnetic permeability and inversely proportional to the magnetic reluctance when the number of coil turns is constant.

The traditional PMSM has a permanent magnet on the d-axis, whose permeability is close to that of air, which is equivalent to air-gap widening on the d-axis and makes the magnetic reluctance of the d-axis higher than q-axis. According to Formula (1), the q-axis reactance is greater than the d-axis reactance. The structure of traditional PMSM is shown in Fig. 1 (a). Realizing the characteristics of $L_d > L_q$ in PMSM means that the d-axis inductance is higher than q-axis inductance. It is necessary to increase the magnetic reluctance on the q-axis magnetic circuit, so trapezoidal ventilation holes should be set up at the q-axis position of the rotor. The structure of reverse salient pole PMSM is shown in Fig. 1 (b).

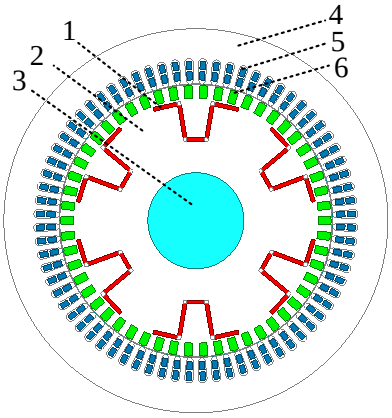

(a)

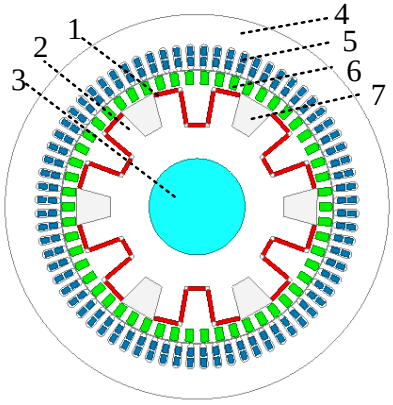

(b)

1-Permanent magnet, 2-Rotor core, 3-Shaft, 4-Stator core, 5-Stator winding, 6-Squirrel cage bar, 7-Ventilated slot

Fig. 1. (a) FEA model of the traditional PMSM, and (b) FEA model of reverse salient pole PMSM

The figures above show the structure of two kinds of motors. In order to accurately compare their performances, the outer and inner diameters of stator and rotor and the amount of permanent magnet are exactly the same. Different from the traditional PMSM, the trapezoidal ventilation holes are formed along the q-axis direction of reverse salient pole PMSM. This makes the flux leakage of the motor less than that of traditional PMSM. The degree of magnetic saturation of q-axis is alleviated and the distribution of magnetic density is more reasonable. As the saturation of magnetic circuit is greatly reduced, the iron loss is reduced and the efficiency of reverse salient pole PMSM is improved. Moreover, ventilation holes can facilitate the rotor heat dissipation, which reduces the rotor temperature and protects the permanent magnet.

III. FEA OF THE REVERSE SALIENT POLE PMSM

In this paper, the FEA software is used to establish the model of the traditional PMSM and the reverse salient pole PMSM. This paper obtains and analyses air-gap flux density waveform, no-load back EMF waveform, d-axis and q-axis inductance characteristics, power angle characteristics and rated load starting performance of the two motors with different structures.

A. Analysis of no-load back EMF and air-gap flux density

The FEA of the traditional PMSM and the reverse salient pole PMSM is carried out. The no-load back EMF and air-gap flux density of the two motors are solved by using the FEA software [8], and the Fourier analysis and the comparison of harmonic component are performed. The no-load back EMF and air-gap flux density waveforms of the two motors are shown in Figs. 2 and 4, respectively.

From Figs. 3 and 5, it can be seen that the fundamental components of no-load back EMF and air-gap flux density of reverse salient pole PMSM increase to a certain extent compared with the traditional PMSM. The fifth and seventh harmonics are also reduced, and the third and ninth harmonics can be suppressed by the Y-connection of the stator windings. Therefore, reverse salient pole PMSM effectively increases the fundamental component and reduces the harmonic component, making back EMF waveform and air-gap flux density waveform closer to sinusoidal wave.

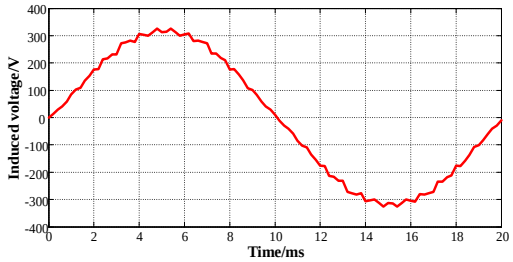

(a)

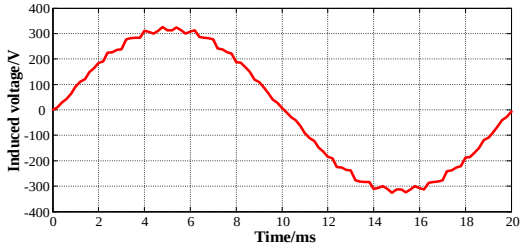

(b)

Fig. 2. (a) No-load back EMF waveform of the traditional PMSM, and (b) no-noad back EMF waveform of reverse salient pole PMSM.

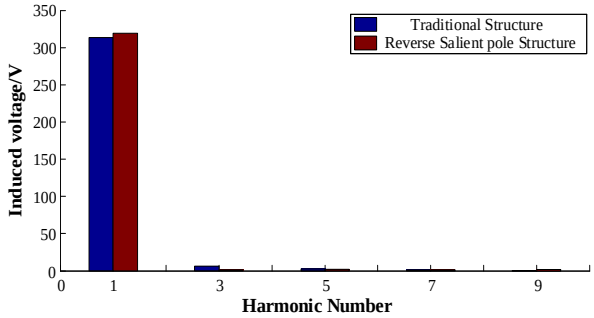

Fig. 3. Harmonic analysis results of no-load back EMF for two kinds of motors.

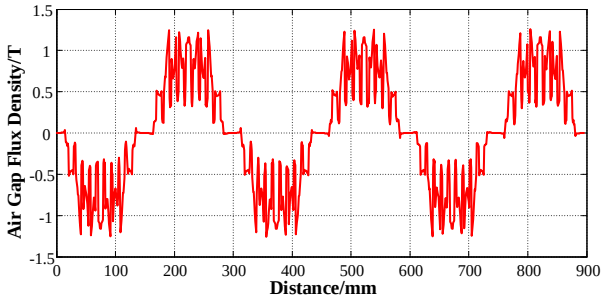

(a)

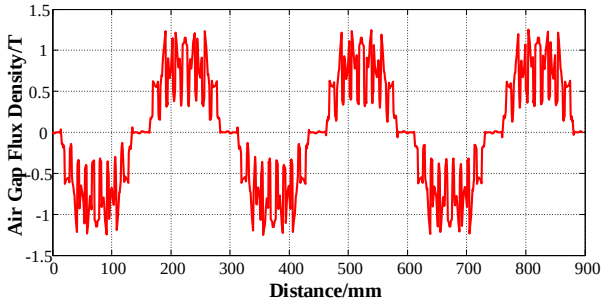

(b)

Fig. 4. (a) Air-gap flux density waveform of the traditional PMSM, and (b) air-gap flux density waveform of reverse salient pole PMSM.

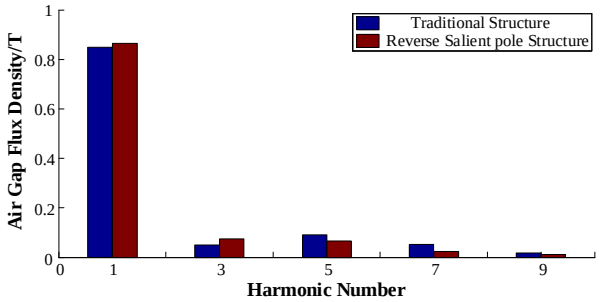

Fig. 5. Harmonic analysis results of air-gap flux density for two kinds of motors.

B. Analysis of inductance characteristics of d-axis and q-axis

The d-axis and q-axis inductances have great influence on the operation characteristics. The reverse salient pole effect of motor is expressed in terms of the parameter $L_d > L_q$. Therefore, it is very important to analyze the inductance characteristics. At present, most inductance calculation methods are based on magnetic circuit method. By introducing some optimum parameters and calculating them according to empirical formulas, the accuracy is not high. When the structure of magnetic circuit is complex, it is difficult to calculate by this method. In this paper, the FEA is used to calculate the reactance of PMSM.

The winding flux linkage of d-axis and q-axis are mutually vertical, but in the actual motor, d-axis and q-axis are not completely decoupled. So there is a strong cross-coupling between them. The expression of flux linkage considering cross-coupling is as follows [9]:

$$\lambda_d=\lambda_d(i_d, i_q)=L_d i_d+L_{dq} i_q+\lambda_f, \quad (2)$$

$$\lambda_q=\lambda_q(i_d, i_q)=L_q i_q+L_{dq} i_d. \quad (3)$$

In the formula, L_d and L_q are the self-inductance of d-axis and q-axis respectively; L_{dq}, L_{qd} are the d-axis and the q-axis mutual inductance; λ_f is the flux linkage of the permanent magnet.

According to the expression of flux linkage shown in formula (2), (3), Aimeng from North China Electric Power University has proposed and revised the calculation model of L_d and L_q considering cross-saturation of magnetic circuit:

$$L_d = \frac{\lambda_d(i_d,i_q)-\lambda_f(0,0)}{i_d}\Big|_{i_q=constant}, \quad (4)$$

$$L_q=\frac{\lambda_q(i_d,i_q)}{i_q}\Big|_{i_d=constant}. \quad (5)$$

The calculation model of inductance parameters shown in formula (4), the flux linkage of permanent magnet is obtained when the stator current is zero. Therefore, in solving the d-axis inductance, the flux that acts only on permanent magnet is subtracted, and the effect of q-axis current on d-axis magnetic circuit is fully considered. According to formulas (4), (5), the FEA method is used to analyze the calculation model of inductance parameters. When calculating d-axis inductance of two kinds of motors, q-axis current is set to the rated value, and d-axis current changes from 5A to 50A. Similarly, when calculating q-axis inductance, d-axis current is set to the rated value, and q-axis current changes from 5A to 50A [10]. Therefore, the inductance characteristics of two motors that fully consider the cross-saturation of the d-axis and q-axis magnetic circuit can be obtained, as is shown in Figures 6 (a) and 6 (b).

It can be seen from Fig. 6 (a) that the traditional PMSM expresses salient pole effect of $L_d > L_q$. Because of the high degree of magnetic saturation, the inductance of d-axis and q-axis decrease obviously with the increase of the current of their respective axis. Moreover, due to the existence of permanent magnets on the d-axis, the saturation degree of the d-axis is less than that of the q-axis, so reduction of the d-axis inductance is less obvious than that of the q-axis inductance. In Fig. 6 (b), due to the trapezoidal ventilation slot on the q-axis, reverse salient pole PMSM expresses the reverse salient pole effect of $L_d > L_q$. In addition, a trapezoidal ventilation slot is opened on the q-axis of the rotor for the motor, which greatly reduces degree of saturation. Thus, with the increase of current, inductance drop of d-axis and q-axis is less than that of the traditional PMSM.

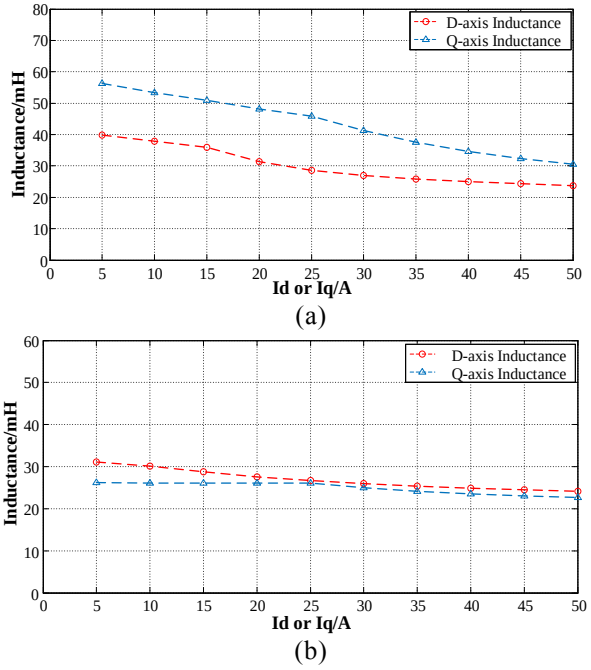

Fig. 6. (a) Inductance curve of the traditional PMSM, and (b) inductance curve of reverse salient pole PMSM.

C. Analysis of power angle characteristics

In order to obtain the power angle characteristics of PMSM, it is necessary to solve the torque. By setting different power angles in the FEA software, the torque values corresponding to different power angles are solved, and the power angle characteristics are obtained.

Generally, the stator winding resistance R_1 is small, neglecting its influence, the torque of the salient pole PMSM is as follows [11]:

$$T_{em}=m\frac{E_0 U}{X_d \Omega_s}\sin\delta+m\frac{U^2}{2\Omega_s}\left(\frac{1}{X_q}-\frac{1}{X_d}\right)\sin 2\delta. \quad (6)$$

In (6), m is phase number, E_0 is no-load EMF, U is power supply voltage, Ω_s is mechanical angular velocity, δ is power angle, X_d and X_q are d-axis and q-axis reactance, respectively.

It can be seen from (6) that the torque consists of two parts: basic electromagnetic torque by the interaction

between the rotor permanent magnet field and the stator magnetic field, which is called the permanent magnet torque; as well as the second one donating reluctance torque caused by the unequal reluctance of d-axis and q-axis. In the traditional PMSM, because the q-axis inductance is larger, the power angle corresponding to the maximum torque is over 90° [12]. In reverse salient pole PMSM, the d-axis inductance is higher, so the power angle corresponding to the maximum torque is less than 90°.The power angle characteristics of the two structural motors are obtained by FEA are shown in Fig. 7.

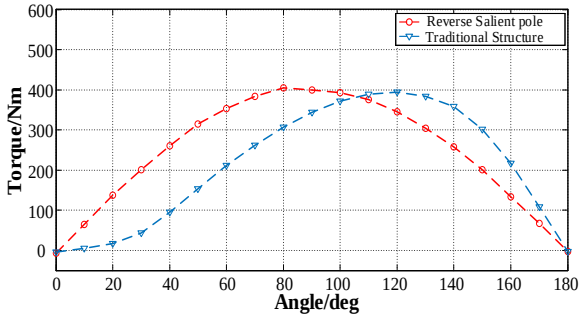

Fig. 7. Power angle characteristics of two kinds of motors.

As can be seen from Fig. 7, different from the power angle characteristic of the traditional PMSM, the maximum torque of reverse salient pole PMSM is at the position where the power angle is at 80 degrees. Therefore, it is known that the reluctance and torque component $T_{em2}=m\frac{U^2}{2\Omega_s}\left(\frac{1}{X_q}-\frac{1}{X_d}\right)sin2\delta$ of the motor is positive when the power angle is less than 90 degrees. It is also proved the reverse salient pole PMSM has reverse salient pole effect of $L_d > L_q$. When the motor operates under load, the magnetic field of the armature reaction in the same direction as the magnetic field of the rotor, which acts as a magnetizing aid. Moreover, compared with the traditional PMSM, the maximum torque of reverse salient pole PMSM increases under the same amount of permanent magnets. It not only improves the utilization ratio of permanent magnet, but also increases the overload capacity [13].

D. Starting performance analysis of rated load

Line-start permanent magnet synchronous motor (LSPMSM) can be regarded as placing permanent magnet in the rotor of three-phase induction motor, which can start by the asynchronous torque generated by the rotor cage winding [14]. The motor has the advantageous ability of self-starting. In this paper, three-phase rated voltage is loaded into three-phase stator windings of two motors by FEA method. In addition, they start at zero speed under rated load (T_N =200N.m). Starting performance of the two motors under rated load are obtained by simulation [15]. Corresponding speed and torque curves are obtained as shown in Figs. 8 and 9.

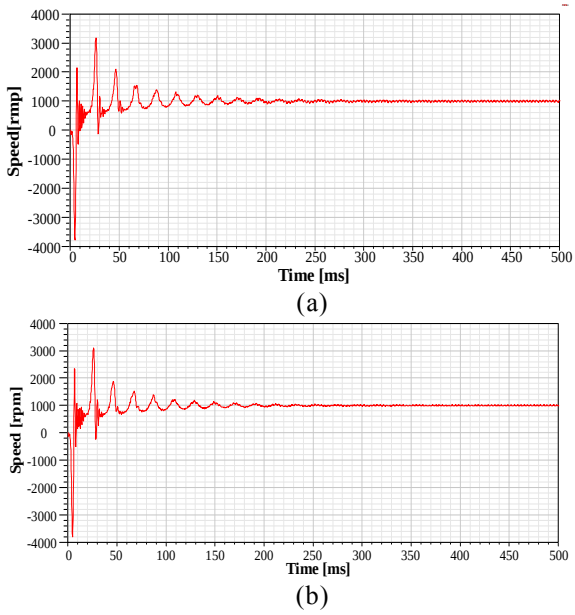

Fig. 8. (a) Starting speed curve of rated load for the traditional PMSM, and (b) starting speed curve of rated load for reverse salient pole PMSM.

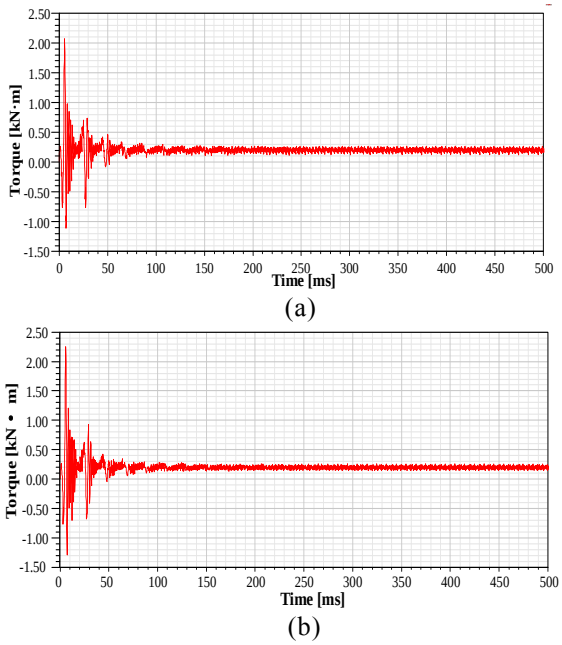

Fig. 9. (a) Starting torque curve of rated load for the traditional PMSM, and (b) starting torque curve of rated load for reverse salient pole PMSM.

Figures 8 and 9 show the speed and torque curves

of the two motors during starting with rated load, respectively. During the process of load starting, the torque is higher in low speed section, and the motor is accelerated close to synchronous speed. After a period of oscillation, it is pulled into synchronous operation. From the speed curve, it can be seen that the speed of the traditional PMSM stabilizes to synchronous speed close to 350*ms*. Speed of reverse salient pole PMSM stabilizes to synchronous speed around 300*ms*. In addition, it can be seen from Figs. 9 (a) and 9 (b) that the torque ripple of the traditional PMSM is more obvious than that of reverse salient pole PMSM in steady-state operation. It shows that the latter is better than the former in starting performance.

E. Efficiency analysis of rated load

Efficiency is an important performance index. When motor operates under load, loss inevitably exists. In this paper, the FEA method is used to obtain the iron loss, stator copper loss and rotor copper loss of two kinds of motors at steady-state operation [16]. As shown in Table 2 below.

Table 2: Efficiency of two kinds of motors under rated load

	The Traditional PMSM	The Teverse Salient Pole PMSM
Iron loss (W)	338.5	318
Stator copper loss (W)	285.7	226
Rotor copper loss (W)	366.6	287.3
Output power (W)	20947.9	20945.6
Efficiency	95.48%	96.18%

As can be seen from Table 2, the efficiency of the two kinds of motor is more than 95%, and the efficiency of reverse salient PMSM is higher than that of the traditional PMSM. The efficiency of the two motors fully meets the requirements of PMSM design. The results show that feasibility and reason of the proposed design.

IV. OPTIMAL DESIGN OF THE REVERSE SALIENT POLE PMSM

Improving fundamental component of air-gap magnetic field and restraining harmonic component are effective ways to improve motor performance. In this paper, a rotor structure with non-uniform teeth is proposed to improve the performance of motor. As shown in Fig. 10, the teeth distance of the rotor at the d-axis position is widened by two times as much as that of the conventional teeth, so that the magnetic reluctance on the d-axis direction decreases, the magnetic density and the fundamental component of the air-gap magnetic field increases.

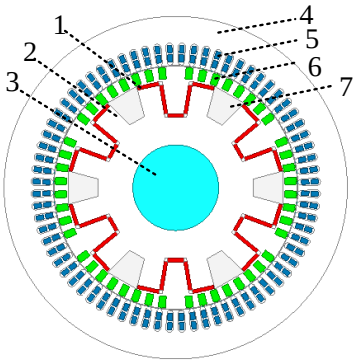

1-Permanent magnet, 2-Rotor core, 3-Shaft, 4-Stator core, 5-Stator winding, 6-Squirrel cage bar, 7-Ventilated slot

Fig. 10. The structure of the optimized reverse salient pole PMSM.

V. FEA OF THE OPTIMIZED REVERSE SALIENT POLE PMSM

In this paper, a model of the optimized reverse salient pole PMSM is established by using FEA software. The FEA simulation is used to obtain air-gap flux density waveform, no-load back EMF waveform, power angle characteristic and rated load starting performance, and then the reverse salient motor described earlier in these main performance is used to compare.

A. Analysis of no-load back EMF and air-gap flux density

The solution of no-load back EMF and air-gap flux density of the optimized reverse salient pole PMSM is carried out by using FEA software. The waveforms are shown in Figs. 11 (a) and 11 (b). At the same time, the no-load back EMF and air-gap flux density are analyzed by Fourier method, and compared with the reverse salient pole PMSM. The results are shown in Figs. 12 and 13.

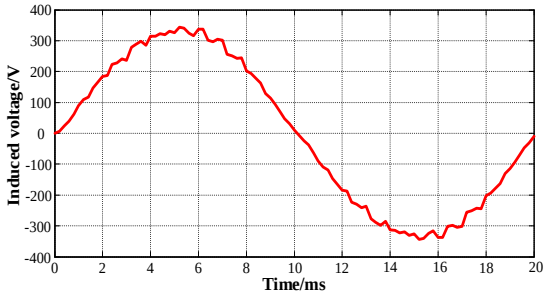

(a)

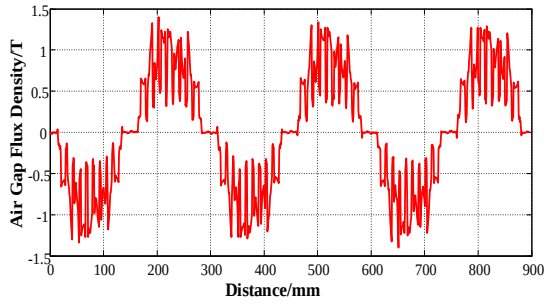

(b)

Fig. 11. (a) No-load back EMF waveform of the optimized reverse salient pole PMSM, and (b) air-gap flux density waveform of the optimized reverse salient pole PMSM.

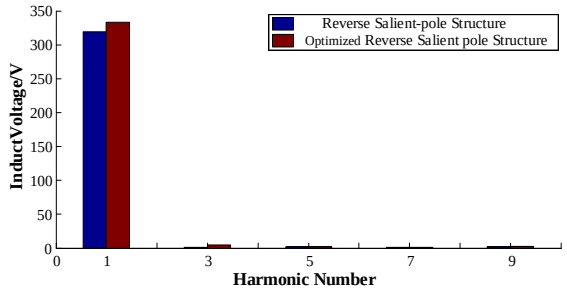

Fig. 12. Harmonic analysis results of no-load back EMF for two kinds of motors.

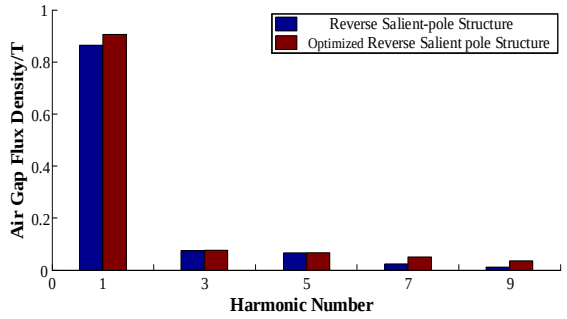

Fig. 13. Harmonic analysis results of air-gap flux density for two kinds of motors.

From Figs. 12 and 13, it can be seen that the fundamental components of no-load back EMF and air-gap flux density of the optimized reverse salient pole PMSM obviously increase compared with reverse salient pole PMSM. The fifth and seventh harmonics are roughly the same, while the third and ninth harmonics are also suppressed. Therefore, the optimized reverse salient pole PMSM effectively increases the fundamental component and reduces the proportion of harmonic components, making the back EMF waveform and air-gap flux density waveform are closer to sinusoidal wave.

B. Analysis of power angle characteristic for the optimized reverse salient pole PMSM

In this paper, the optimized reverse salient pole PMSM is set different power angles by FEA software, and the corresponding torque values are solved to obtain its power angle characteristics. Compared with the power angle characteristic of reverse salient pole PMSM, the results are shown in Fig. 14.

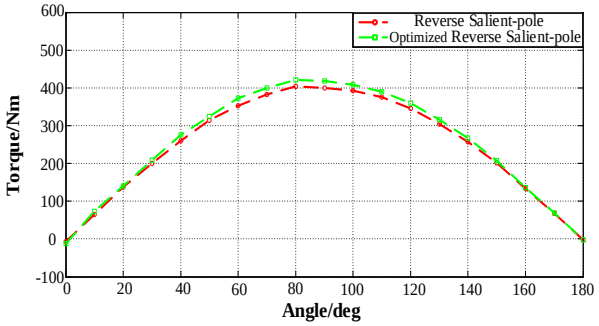

Fig. 14. Power angle characteristics of two kinds of motors.

As can be seen from Fig. 14, the trend of power angle characteristics of the optimized reverse salient pole PMSM are basically the same as that of reverse salient pole PMSM. Because the optimized reverse salient pole PMSM removes six squirrel cage bars on d-axis, which enlarges the width of the rotor teeth and increases the magnetic flux of the motor. Thus, in the case of the same amount of permanent magnets, the torque corresponding to each power angle of the optimized reverse salient pole PMSM will be greater than that of reverse salient pole PMSM, which improves the overload capacity of the motor. Therefore, it is shown that the optimized reverse salient pole PMSM has better performance in the torque.

C. Starting performance analysis of the optimized reverse salient pole PMSM

In this paper, three-phase rated voltage is loaded into three-phase stator windings of the optimized reverse salient pole PMSM. In addition, it also starts at zero speed under rated load (T_N=200N.m). The speed and torque curves of the motor during rated load are obtained by simulation, which is shown in Figs. 15 (a) and 15 (b) below.

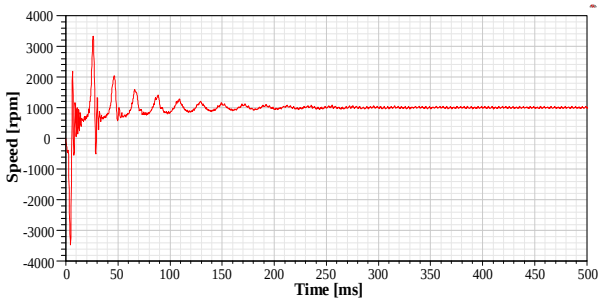

(a)

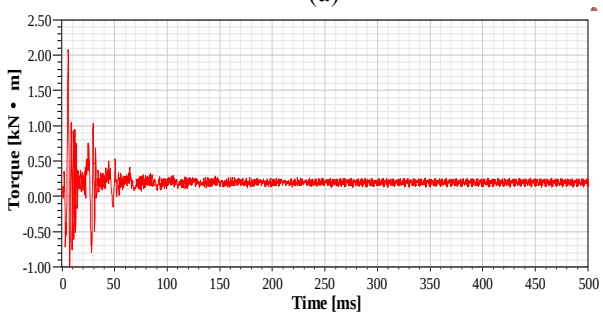

(b)

Fig. 15. (a) Starting speed curve of rated load for the optimized reverse salient pole PMSM, and (b) starting torque curve of rated load for the optimized reverse salient pole PMSM.

From the speed and torque curves, it can be seen that the optimized reverse salient pole PMSM has reached the synchronous speed near 300ms. After reducing six squirrel cage bars of the rotor starting winding, the starting performance of the motor is not affected, which shows the superiority of the starting performance of the optimized reverse salient pole PMSM.

D. Efficiency analysis of the rated load

In this paper, the FEA method is used to simulate the iron loss, stator copper loss and rotor copper loss of the optimized reverse salient pole PMSM during steady-state operation, and compare with reverse salient pole PMSM. The results are shown in Table 3 below.

Table 3: Efficiency of two kinds of motor under rated load

	The Optimized Reverse Salient Pole PMSM	The Reverse Salient Pole PMSM
Iron loss (W)	270.9	318
Stator copper loss (W)	267.7	226
Rotor copper loss (W)	279	287.3
Output power (W)	20949.2	20945.6
Efficiency	96.24%	96.18%

From Table 3, it can be seen that the efficiency of the two kinds of motors is over 96%. Moreover, the efficiency of the optimized reverse salient PMSM is slightly higher than that of the reverse salient PMSM which shows the superiority in efficiency and proves the rationality of the optimized design.

VI. CONCLUSION

In this paper, a novel reverse salient pole PMSM is proposed and optimized. Two-dimensional models of PMSM with three different rotor structures are established and simulated by FEA software. The results show that air-gap flux density and back EMF of reverse salient pole PMSM are closer to sinusoidal wave than those of the traditional PMSM. By opening trapezoidal slots on the q-axis of the rotor, it has reverse salient pole effect of $L_d > L_q$, reducing the risk of demagnetization and increasing operation stability. The reverse salient pole PMSM improves the maximum torque and the overload capacity of the motor. In addition, reverse salient pole PMSM has higher efficiency at rated load. Moreover, the optimized reverse salient pole PMSM in these performances will be better than reverse salient pole PMSM. It also proves the rationality of reverse salient pole PMSM and its optimal design.

ACKNOWLEDGMENT

This work has been supported by the Top-notch Academic Programs Project of Jiangsu Higher Education Institutions PPZY2015B132 and the National Natural Science Foundation of China (U1610113).

REFERENCES

[1] R. Y. Tang, *Modern Permanent Magnet Machines Theory and Design*. Beijing: China Machine Press, 1997, pp. 37-87.

[2] Y. G. Chen, W. G. Zhong, and Y. H. Shen, "Finite element analysis of interior composite-rotor controllable flux permanent magnet synchronous machine," *Proceedings of the CSEE*, vol. 29, no. 6, pp. 61-66, Feb. 2009.

[3] G. Kang, Y. Son, G. Kim, and J. Hur, "A novel cogging torque reduction method for interior-type permanent-magnet motor," *IEEE Transactions on Industry Applications*, vol. 45, no. 1, pp. 161-167, Jan.-Feb. 2009.

[4] N. Limsuwan, Y. Shibukawa, D. D. Reigosa, and R. D. Lorenz, "Novel design of flux-intensifying interior permanent magnet synchronous machine suitable for self-sensing control at very low speed and power conversion," *IEEE Transactions on Industry Applications*, vol. 47, no. 5, pp. 2004-2012, Sept.-Oct. 2011.

[5] N. Limsuwan, T. Kato, K. Akatsu, and R. D. Lorenz, "Design and evaluation of a variable-

flux flux-intensifying interior permanent-magnet machine," *IEEE Trans. Ind. Appl.*, vol. 50, no. 2, pp. 1015-1024, Mar./Apr. 2014.

[6] X. Zhu, S. Yang, Y. Du, Z. Xiang, and L. Xu, "Electromagnetic performance analysis and verification of a new flux-intensifying permanent magnet brushless motor with two-layer segmented permanent magnets," *IEEE Transactions on Magnetics*, vol. 52, no. 7, pp. 1-4, July 2016.

[7] X. Zhu, J. Huang, L. Quan, Z. Xiang, and B. Shi, "Comprehensive sensitivity analysis and multi-objective optimization research of permanent magnet flux-intensifying motors," *IEEE Transactions on Industrial Electronics*, vol. 66, no. 4, pp. 2613-2627, Apr. 2019.

[8] A. Mahmoudi, S. Kahourzade, A. A. Rahim, W. P. Hew, and M. N. Uddin, "Design, analysis, and prototyping of a novel structured solid rotor ringed line-start axial-flux permanent magnet motor," *IEEE Trans. Ind. Electron.*, vol. 61, no. 4, pp. 1722-1734, Apr. 2014.

[9] A. Hassanpour Isfahani and S. Vaez-Zadeh, "Effects of magnetizing inductance on start-up and synchronization of line-start permanent-magnet synchronous motors," *IEEE Transactions on Magnetics*, vol. 47, no. 4, pp. 823-829, Apr. 2011.

[10] D. Mingardi, M. Morandin, S. Bolognani, and N. Bianchi, "On the proprieties of the differential cross-saturation inductance in synchronous machines," *IEEE Transactions on Industry Applications*, vol. 53, no. 2, pp. 991-1000, Mar-Apr. 2017.

[11] D. Stoia, M. Cernat, A. A. Jimoh, and D. V. Nicolae, "Analytical design and analysis of line-start permanent magnet synchronous motors," *AFRICON 2009*, Nairobi, pp. 1-7, 2009.

[12] R. T. Ugale and B. N. Chaudhari, "A new rotor structure for line start permanent magnet synchronous motor," *2013 International Electric Machines & Drives Conference*, Chicago, IL, pp. 1436-1442, 2013,.

[13] L. Wang, X. Deng, J. Lu, K. Wang, and R. Wang, "Design and finite element analysis of permanent magnet synchronous motor with novel rotor type," *2010 Asia-Pacific Power and Energy Engineering Conference*, Chengdu, pp. 1-4, 2010.

[14] W. Fei, P. C. K. Luk, J. Ma, J. X. Shen, and G. Yang, "A high-performance line-start permanent magnet synchronous motor amended from a small industrial three-phase induction motor," *IEEE Transactions on Magnetics*, vol. 45, no. 10, pp. 4724-4727, Oct. 2009.

[15] R. T. Ugale and B. N. Chaudhari, "Rotor configurations for improved starting and synchronous performance of line start permanent-magnet synchronous motor," *IEEE Transactions on Industrial Electronics*, vol. 64, no. 1, pp. 138-148, Jan. 2017.

[16] M. J. Melfi, S. D. Umans, and J. E. Atem, "Viability of highly efficient multi-horsepower line-start permanent-magnet motors," *IEEE Transactions on Industry Applications*, vol. 51, no. 1, pp. 120-128, Jan.-Feb. 2015.

Xianming Deng was born in Sichuan, China. He received his B.S., M.S., and Ph.D. in Electrical Engineering from China University of Mining and Technology, Jiangsu, China. He is currently a Professor in the School of Electrical and Power Engineering of China University of Mining and Technology. His current research fields include power electronics and motor drive.

Shusheng Gong was born in Fujian, China. He received his B.S. in Electrical Engineering from Fujian Agriculture and Forestry University, Fujian, China. He is currently receiving a Master education at China University of Mining and Technology. His current research directions include motor design and motor control.

Ran Li was born in Shanxi, China. He received his B.S. in Electrical Engineering from Shandong University of Technology, Shandong, China. He is currently receiving a Master education at China University of Mining and Technology. His current research interests include power electronics and motor drive.

Junhong Zhou was born in Hunan, China. He received his B.S. in Information Engineering from China University of Mining and Technology, Jiangsu, China. He is currently receiving a Master education at China University of Mining and Technology. His current research interests include power electronics and motor drive.